




**Antiskyrmions and Bloch skyrmions in magnetic Dresselhaus metals**Deepak S. Kathyat , Arnob Mukherjee , and Sanjeev Kumar *Department of Physical Sciences, Indian Institute of Science Education and Research Mohali,  
Sector 81, S.A.S. Nagar, Manauli PO 140306, India*

(Received 8 July 2021; revised 5 November 2021; accepted 17 November 2021; published 30 November 2021)

We present a microscopic electronic description of how antiskyrmions can be stabilized in a Dresselhaus spin-orbit-coupled magnetic metal. Furthermore, we show that the antiskyrmions can be tuned into Bloch skyrmions via a change in sign of the hopping integral. The results are based on the state-of-the-art hybrid Monte Carlo simulations of lattice models explicitly involving itinerant electrons. The origin of such topological textures is understood via an effective spin-only model. Our results uncover an important and useful connection between generic features of the band structure and topological spin textures of immense current interest, and present a microscopic explanation of skyrmion formation reported recently in certain magnetic Weyl semimetals.

DOI: [10.1103/PhysRevB.104.184434](https://doi.org/10.1103/PhysRevB.104.184434)**I. INTRODUCTION**

The importance of magnetic skyrmion and antiskyrmion (ASk) quasiparticles in future technologies has been very well accepted [1–5]. Consequently, identifying new materials that host such exotic magnetic textures has become a highly active and important area of research. The appearance of skyrmions has been confirmed with small angle neutron scattering and Lorentz transmission electron microscopy measurements in bulk as well as in thin films of a variety of chiral magnets [6–14]. On the other hand, while there are a few reports of their existence in thin-film samples, antiskyrmions have been mostly observed in bulk materials [15–19]. Interestingly, the disappearance of antiskyrmions in the thinner region of samples of  $D_{2d}$  Heusler materials has also been reported [15]. While the early theoretical understanding of these textures was largely based on phenomenological magnetic models, recent years witnessed efforts towards a microscopic electronic description of these topological textures [20–25]. Most of these recent studies focused on identifying the correct electronic model to stabilize one specific type of magnetic textures, such as, Neel- or Bloch-skyrmions or antiskyrmions.

The role of Dzyaloshinskii-Moriya (DM) interactions in stabilizing skyrmion-like textures is also well documented [26–30]. Current theories suggest that, while skyrmions are stabilized by isotropic DM coupling, the stabilization of antiskyrmions require anisotropic DM interactions [19,31,32] or dipolar interactions [33]. At a more fundamental level, the DM interactions emerge from the spin-orbit coupling (SOC), which can be of atomic, Rashba, or Dresselhaus type. Recent investigations clarified how even in metallic systems, where the itinerant nature of electrons plays a crucial role, the Rashba-type SOC generates terms that resemble the DM interactions. This has led to an elementary understanding of the formation of Neel-type skyrmions in magnetic metals that support a moderate strength of Rashba SOC [34,35]. However, a large number of magnetic metals with broken inversion symmetry are known to host Bloch-type skyrmions. In

addition to a phenomenological understanding, microscopic theories based on geometrical frustration can also explain the formation of Bloch skyrmions [36]. However, not all materials that exhibit Bloch-skyrmion signatures possess a geometrically frustrated magnetic lattice. Furthermore, most of these materials are metals where a microscopic picture ignoring electronic itinerancy is highly questionable. The existence of skyrmions has also been experimentally inferred in magnetic Weyl semimetals, which show nodal-point structure in the electronic bands as well as magnetic ordering [37–40]. Properties of the Weyl electrons in such materials can get enriched in the presence of skyrmion-like magnetic textures in real space. The microscopic mechanism for the formation of these textures in Weyl semimetals is currently unknown.

In this work, we show that the Dresselhaus double exchange (DDE) model microscopically describes the formation of antiskyrmions. We study the model on a square lattice via state-of-the-art hybrid Monte-Carlo (HMC) simulations. We find that the DDE model in the presence of Zeeman coupling to an external magnetic field stabilizes antiskyrmion textures. We then show that a simple change in sign of one of the hopping parameters converts antiskyrmions into Bloch skyrmions. This is physically relevant as many of the magnetic materials hosting Bloch skyrmions display the minimum location away from the  $\Gamma$  point confirming a relative sign-difference between hopping parameters along different directions [41–44]. An effective spin-model is studied for a conventional understanding of these results. We further establish a connection between the DDE model and the magnetic Weyl semimetals, thereby explaining the recent experimental observations of skyrmions in the semimetals.

**II. ANTISKYRMIONS IN A MODEL FOR DRESSELHAUS MAGNETIC METALS**

As a prototype of metallic magnets that lack inversion center in their structure, we consider a tight-binding model with Dresselhaus SOC and Hund's coupling on a square lattice.

The Hamiltonian is given by

$$H = -t \sum_{\langle ij \rangle, \sigma} (c_{i\sigma}^\dagger c_{j\sigma} + \text{H.c.}) + \lambda \sum_i [i(c_{i\downarrow}^\dagger c_{i+x\uparrow} + c_{i\uparrow}^\dagger c_{i+x\downarrow}) + (c_{i\downarrow}^\dagger c_{i+y\uparrow} - c_{i\uparrow}^\dagger c_{i+y\downarrow}) + \text{H.c.}] - J_H \sum_i \mathbf{S}_i \cdot \mathbf{s}_i. \quad (1)$$

Here,  $c_{i\sigma}$  ( $c_{i\sigma}^\dagger$ ) annihilates (creates) an electron at site  $i$  with spin  $\sigma$ ,  $\langle ij \rangle$  implies that  $i$  and  $j$  are nearest-neighbor (nn) sites. The strengths of hopping and Dresselhaus SOC are denoted, respectively, by  $t$  and  $\lambda$ . The last term describes a coupling between electronic spin  $\mathbf{s}_i$  and localized core spins  $\mathbf{S}_i$ . In many material involving Mn, Fe, or rare-earth ions a well-localized core spin explicitly exists, and therefore the last term is justified. However, the scope of this term is broader since the Hubbard model at the mean-field level also generates an effective Hund's coupling [45,46]. We parametrize  $t = (1 - \alpha)t_0$  and  $\lambda = \alpha t_0$  and set  $t_0 = 1$  as the reference energy scale. This parametrization turns out to be useful in connecting the extreme limits of vanishing SOC and vanishing hopping [34]. For a given  $\alpha$ , we can readily obtain the more commonly used parameter  $\lambda/t = \alpha/(1 - \alpha)$ . Assuming large  $J_H$  and taking the double-exchange approximation, we obtain the DDE Hamiltonian

$$H_{\text{DDE}} = \sum_{\langle ij \rangle, \gamma} [g_{ij}^\gamma d_i^\dagger d_j + \text{H.c.}] - h_z \sum_i S_i^z, \quad (2)$$

where  $d_i$  ( $d_i^\dagger$ ) annihilates (creates) an electron at site  $i$  with spin parallel to the localized spin. The Zeeman coupling of spins to an external magnetic field of strength  $h_z$  was also included in Eq. (2). Site  $j = i + \gamma$  is the nn of site  $i$  along spatial direction  $\gamma = x, y$ . The projected hopping  $g_{ij}^\gamma = t_{ij}^\gamma + \lambda_{ij}^\gamma$  depends on the orientations of the local moments  $\mathbf{S}_i$  and  $\mathbf{S}_j$ ,

$$\begin{aligned} t_{ij}^\gamma &= -t \left[ \cos\left(\frac{\theta_i}{2}\right) \cos\left(\frac{\theta_j}{2}\right) + \sin\left(\frac{\theta_i}{2}\right) \sin\left(\frac{\theta_j}{2}\right) e^{-i(\phi_i - \phi_j)} \right], \\ \lambda_{ij}^x &= i\lambda \left[ \sin\left(\frac{\theta_i}{2}\right) \cos\left(\frac{\theta_j}{2}\right) e^{-i\phi_i} + \cos\left(\frac{\theta_i}{2}\right) \sin\left(\frac{\theta_j}{2}\right) e^{i\phi_j} \right], \\ \lambda_{ij}^y &= \lambda \left[ \sin\left(\frac{\theta_i}{2}\right) \cos\left(\frac{\theta_j}{2}\right) e^{-i\phi_i} - \cos\left(\frac{\theta_i}{2}\right) \sin\left(\frac{\theta_j}{2}\right) e^{i\phi_j} \right], \end{aligned} \quad (3)$$

where  $\theta_i$  ( $\phi_i$ ) denotes the polar (azimuthal) angle for localized spin  $\mathbf{S}_i$ .

We study the DDE Hamiltonian using numerically exact HMC simulations [35,47,48]. The presence of skyrmions or antiskyrmions is inferred via local skyrmion density [26]

$$\chi_i = \frac{1}{8\pi} [\mathbf{S}_i \cdot (\mathbf{S}_{i+x} \times \mathbf{S}_{i+y}) + \mathbf{S}_i \cdot (\mathbf{S}_{i-x} \times \mathbf{S}_{i-y})]. \quad (4)$$

Total skyrmion density is defined as  $\chi = \sum_i \chi_i$ . We also compute the relevant component of vector chirality  $\eta$  as

$$\eta = \frac{1}{N} \sum_i (\mathbf{S}_i \times \mathbf{S}_{i+y}) \cdot \hat{y} - (\mathbf{S}_i \times \mathbf{S}_{i+x}) \cdot \hat{x}. \quad (5)$$

The results obtained via HMC simulations for two representative values of  $\alpha$ , at electronic filling of  $n = 0.3$ , are shown in Fig. 1. The existence of antiskyrmions in the DDE Hamiltonian is explicitly demonstrated via the spin configurations [see Figs. 1(a) and 1(c)] as well as skyrmion

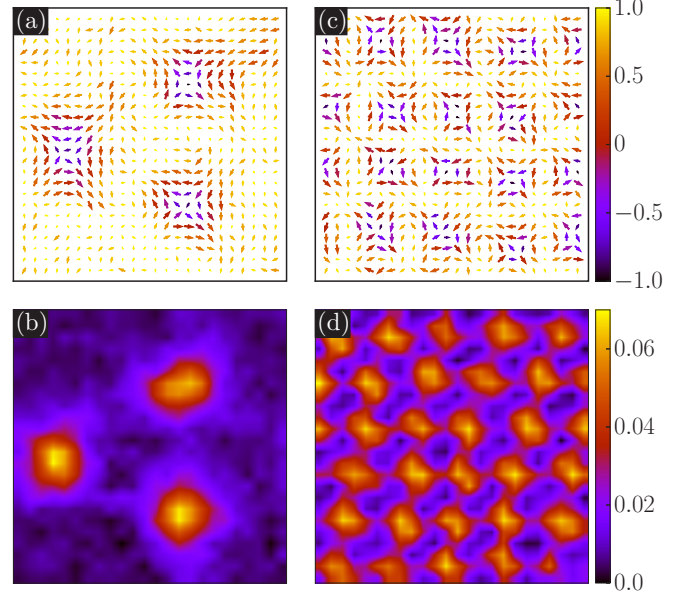


FIG. 1. (a,c) Snapshots of spin configurations and (b,d) the local skyrmion density at  $T = 0.01$  for representative values of  $\alpha$  and  $h_z$  as obtained in HMC simulations: (a,b)  $\alpha = 0.25$ ,  $h_z = 0.03$ ; (c,d)  $\alpha = 0.4$ ,  $h_z = 0.06$ . The HMC simulations are performed on  $24 \times 24$  lattice for an average band filling fraction of 0.3.

density maps [see Figs. 1(b) and 1(d)] at low temperatures representative of the ground states. The positive sign of  $\chi$  that is opposite to the sign of the polarity (defined by magnetization of the central spin of the texture) reveals that the ground states are antiskyrmions. We find that small values of  $\alpha$  lead to sparse antiskyrmions within the zero-field-cooled (ZFC) protocol and the packing (size) of antiskyrmions increases (decreases) with increasing  $\alpha$ . Note that the Hamiltonian Eq. (2) does not contain any direct spin-spin interaction terms. Therefore, the magnetic patterns discussed above are stabilized by interactions that are mediated via conduction electrons. A conventional understanding of the formation of such textures can only emerge via identification of the emergent spin-spin interactions in this model. To this end, we now present results on an effective spin-only model derived from the DDE Hamiltonian.

### III. ANTISKYRMIONS IN THE EFFECTIVE SPIN MODEL

We derive an effective spin model for  $H_{\text{DDE}}$  in close analogy to the derivation of  $H_{\text{RDE}}$  in [35]. The resulting effective model is given by

$$H_{\text{eff}} = - \sum_{\langle ij \rangle} D_{ij}^{x(y)} f_{ij}^{x(y)} - h_z \sum_i S_i^z, \quad (6)$$

where the functional dependence on classical spin variables is contained in the modulus  $f_{ij}^{x(y)}$  of the complex number  $g_{ij}^{x(y)}$  appearing in Eq. (2). This is specified by

$$\begin{aligned} \sqrt{2} f_{ij}^{x(y)} &= [t^2 \{1 + \mathbf{S}_i \cdot \mathbf{S}_j\} - (+) 2t\lambda \hat{x}(\hat{y}) \cdot \{\mathbf{S}_i \times \mathbf{S}_j\} \\ &\quad + \lambda^2 \{1 - \mathbf{S}_i \cdot \mathbf{S}_j + 2\{\hat{x}(\hat{y}) \cdot \mathbf{S}_i\} \{\hat{x}(\hat{y}) \cdot \mathbf{S}_j\}\}]^{1/2}. \end{aligned} \quad (7)$$

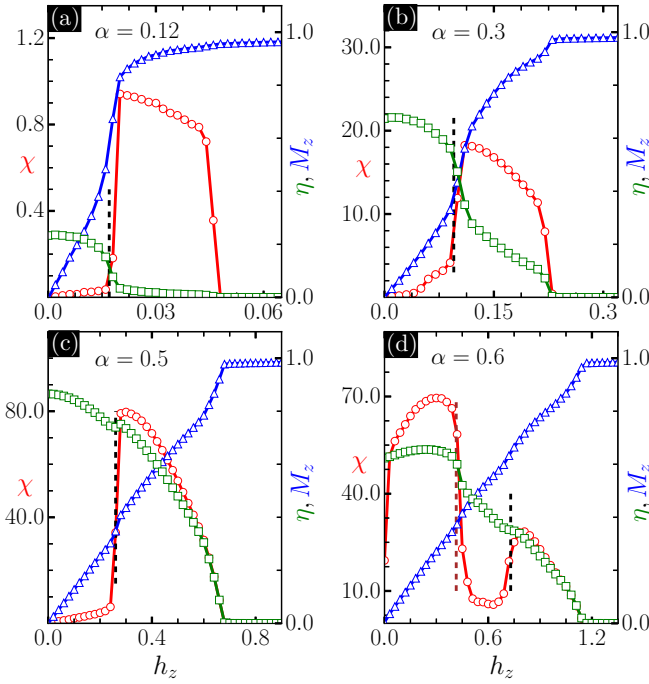


FIG. 2. (a)–(d) Variation of magnetization  $M_z$  (triangles), total skyrmion density  $\chi$  (circles), and vector chirality  $\eta$  (squares) with increasing  $h_z$  for different values of  $\alpha$  at  $T = 0.01$ .

It has been shown that using a constant value of  $D_{ij}^{x(y)}$  captures the essential physics of the Hamiltonian Eq. (6), therefore we set  $D_{ij}^{x(y)} \equiv D_0 = 1$  and simulate  $H_{\text{eff}}$  using the conventional classical MC [34,35]. The first term on the right-hand side inside the square-root in the definition of  $f_{ij}^{x(y)}$  is an isotropic term favoring ferromagnetic ordering. The second term is an anisotropic DM-like exchange coupling of strength  $-2t\lambda$  ( $+2t\lambda$ ) along the  $x$  ( $y$ ) direction and the last term is a pseudodipolar term that leads to magnetic ground-state degeneracy of nongeometrical origin.

In Fig. 2 we show the field dependence of magnetization  $M_z = \frac{1}{N} \sum_i S_i^z$ , vector chirality  $\eta$ , and skyrmion density  $\chi$  obtained via simulations of  $H_{\text{eff}}$  Eq. (6). For small values of  $\alpha$ , a linear increase of magnetization for small  $h_z$ , is followed by a nonlinear behavior that is accompanied by a sharp increase in  $\chi$  [see Figs. 2(a) and 2(b)]. We can infer that the emergence of antiskyrmions makes it difficult for spins to align along the direction of the external magnetic field. The existence of a finite  $\eta$  in the absence of magnetic field can be understood from the DM-like terms in  $H_{\text{eff}}$ . Upon increasing  $h_z$ ,  $\eta$  displays a sharp decrease concomitant with the increase in  $\chi$  [see Figs. 2(a) and 2(b)]. Finally, as the system approaches a field-enforced saturated FM state, both  $\chi$  and  $\eta$  vanish. For  $\alpha = 0.5$ , the change in  $\chi$  near  $h_z = 0.25$  is accompanied by a weak discontinuity in both  $M_z$  and  $\eta$  [see Fig. 2(c)]. This qualitatively different behavior is an indicator of packed ASk state, as will be illustrated below with the help of real space spin configurations. For  $\alpha = 0.6$ ,  $\chi$  is finite even at  $h_z = 0$  indicating the existence of a zero-field antiskyrmion crystal state. A sharp reduction in  $\chi$  near  $h_z = 0.4$  indicates the destabilization of this low-field ASk state. At higher fields a qualitatively different finite-field ASk state appears. The

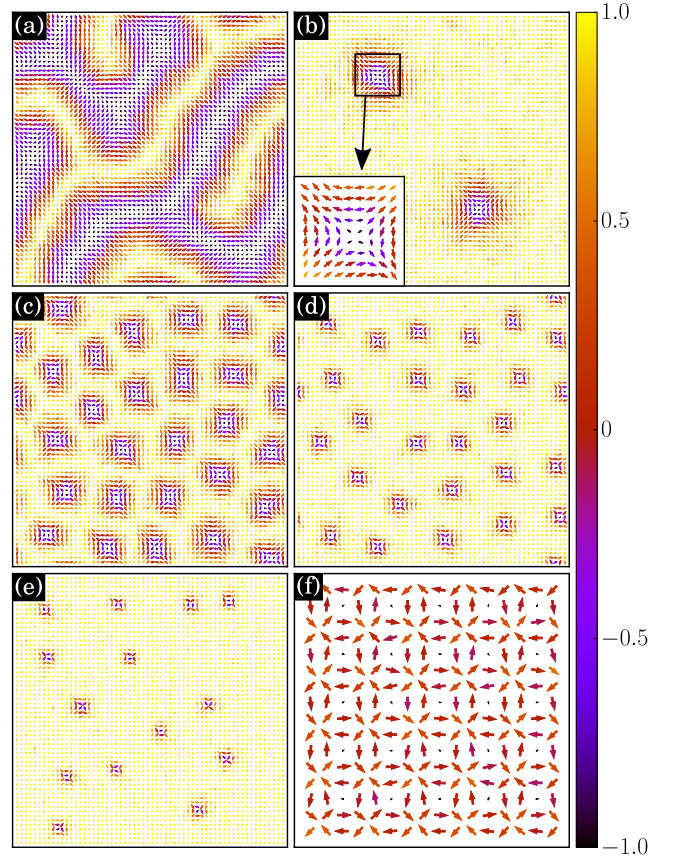


FIG. 3. Snapshots of spin configurations at  $T = 0.01$  for representative values of  $\alpha$  and  $h_z$ . (a) Filamentary domain walls at  $\alpha = 0.15$ ,  $h_z = 0$ , (b) sparse antiskyrmions at  $\alpha = 0.15$ ,  $h_z = 0.036$ , (c) packed antiskyrmions at  $\alpha = 0.3$ ,  $h_z = 0.11$ , (d) ASk size reduction at  $\alpha = 0.3$ ,  $h_z = 0.18$  w.r.t. (c), (e) ASk number reduction at  $\alpha = 0.3$ ,  $h_z = 0.22$  w.r.t. (d), (f) The zero-field ASk crystal at  $\alpha = 0.6$ . For (a)–(e)  $60 \times 60$  lattices are shown. For (f) a smaller section,  $16 \times 16$  of the full lattice is shown for clarity. The color bar corresponds to the  $z$  component of spins.

transition to this high-field phase is identified from the abrupt rise in  $\chi$  near  $h_z = 0.75$  [see Fig. 2(d)]. This antiskyrmion phase is similar to the sparse skyrmion phase discussed in detail in a previous study [35].

We show in Fig. 3 the evolution of magnetic textures with change in  $\alpha$  and  $h_z$  within  $H_{\text{eff}}$ . Within the ZFC protocol at finite temperatures, we find states with filamentary domain wall structure characterized by the diffuse ring pattern in the spin structure factor [34,35] in the absence of external field for small  $\alpha$  [see Fig. 3(a)]. The filamentary domain walls are randomly oriented and look similar to those reported in the Rashba model [34]. However, unlike Rashba systems wherein a spiral in  $xz$  ( $yz$ ) plane is preferred along the  $x$  ( $y$ ) direction, in Dresselhaus metals a spiral in an  $xz$  ( $yz$ ) plane along the  $y$  ( $x$ ) direction is favored. These states can be viewed as the parent state for the antiskyrmions when magnetic field is applied [see Fig. 3(b)]. For larger values of  $\alpha$ , the SQ spiral state gives way to the packed ASk phase [see Fig. 3(c)]. For a given  $\alpha$ , increasing  $h_z$  leads to a reduction of the size by polarizing the spins at the edges of skyrmions [compare Figs. 3(c) and

3(d)], followed by a reduction in the number of antiskyrmions [compare Figs. 3(d) and 3(e)]. A perfectly ordered crystal of smallest possible antiskyrmions on a square lattice is obtained in the absence of external field at  $\alpha = 0.6$  [see Fig. 3(f)]. This value of  $\alpha$  corresponds to a very strong SOC given by  $\lambda/t = 1.5$ . While a SOC comparable to bandwidth seems unrealistic, it may still be effectively realized in flat-band systems where the bandwidth itself is very low. In this limit, the energy term is dominated by the pseudodipolar ( $2\{\hat{x}(\hat{y}) \cdot \mathbf{S}_i\}\{\hat{x}(\hat{y}) \cdot \mathbf{S}_j\}$ ) terms associated with  $\lambda^2$  [see Eq. (7)]. This pseudodipolar term favors axial spin spiral states. Consequently, the square arrangement of two skyrmions can be understood as a superposition of two energetically degenerate spin spirals of wave vectors  $(Q, 0)$  and  $(0, Q)$ .

It is a common practice to describe the skyrmion formation with the help of phenomenological continuum free-energy functionals [27,49–52]. The results discussed in our study are, instead, based on a fully microscopic electronic model. The mechanism for formation of skyrmions in our model does not rely on the presence of various anisotropies that are commonly used in free-energy functionals and spin models [26,51]. As expected, we find that the antiskyrmion sizes become smaller upon increasing the strength of SOC. In the small  $\alpha$  limit, the term proportional to  $\lambda^2$  in the effective Hamiltonian Eq. (7) becomes negligible and the leading correction to ferromagnetism is contained in the DM-like term proportional to  $t\lambda$ . Therefore, we expect that the results in the small  $\alpha$  limit will approach those obtained within continuum models [49–52]. This is already seen in our simulations for  $\alpha = 0.12$  [see Fig. 2(d)]. However, given that one requires much larger lattice sizes to accommodate larger antiskyrmions, we are not able to explicitly check the limit of very small  $\alpha$  in the present study.

#### IV. TURNING ANTISKYRMIONS INTO BLOCH SKYRMIONS

Our results so far show that antiskyrmions exist in Dresselhaus metals and Neel-type skyrmions in Rashba metals [35]. However, Bloch-type skyrmions were reported in many magnetic metals. Our description will certainly remain incomplete if we cannot show the formation of Bloch-type skyrmions within our microscopic model. We now discuss an elegant and physically relevant mechanism to turn antiskyrmions into Bloch skyrmions.

The introduction of a relative sign between the  $x$  and  $y$  direction hopping parameter modifies the  $f_{ij}'$  of the effective Hamiltonian Eqs. (6) and (7) as follows:

$$\sqrt{2}f_{ij}' = [t^2(1 + \mathbf{S}_i \cdot \mathbf{S}_j) + 2t\lambda\hat{\gamma} \cdot (\mathbf{S}_i \times \mathbf{S}_j) + \lambda^2(1 - \mathbf{S}_i \cdot \mathbf{S}_j + 2(\hat{\gamma} \cdot \mathbf{S}_i)(\hat{\gamma} \cdot \mathbf{S}_j))]^{1/2}, \quad (8)$$

where,  $\hat{\gamma} \in \{x, y\}$ . Please note that the relative hopping sign along the  $x$  and  $y$  directions is unlikely to be reversed within the same system. Therefore, the results discussed in this section highlight how systems with different relative hopping signs will lead to distinct textures even if the nature of spin-orbit coupling is identical. We simulate the modified  $H_{\text{eff}}$  Eq. (8) using the conventional classical MC. In Fig. 4 we show the evolution of magnetic textures with change in  $\alpha$  and  $h_z$

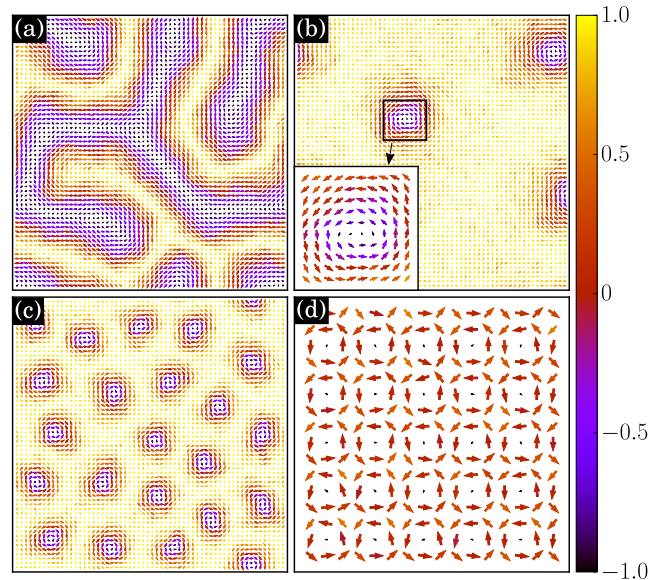


FIG. 4. Low-temperature ( $T = 0.01$ ) snapshots of ground states in modified model for representative values of  $\alpha$  and  $h_z$ . (a) Filamentary domain wall state at  $\alpha = 0.16$ ,  $h_z = 0$ , (b) sparse Bloch skyrmions at  $\alpha = 0.16$ ,  $h_z = 0.036$ , (c) packed Bloch skyrmions at  $\alpha = 0.3$ ,  $h_z = 0.12$ , and (d) Bloch skyrmions crystal at  $\alpha = 0.6$ ,  $h_z = 0.0$ .

within modified  $H_{\text{eff}}$ . We find that, the domain junctions in the filamentary domain wall states for small  $\alpha$  [see Fig. 4(a)] become nucleation centers for Bloch skyrmions when magnetic field is applied [see Fig. 4(b)]. For larger values of  $\alpha$ , packed Bloch skyrmion phase [see Fig. 4(c)] is stabilized as the ground state. While the packed Bloch skyrmions exist in the presence of external field, at  $\alpha = 0.6$  the square-lattice Bloch SkX is the ground state already at  $h_z = 0$  [see Fig. 4(d)]. In summary, the evolution of the phases remains the same as that discussed in previous section for antiskyrmions and the nature of textures gets converted into Bloch-type skyrmions. It is also important to note that in some materials skyrmions and antiskyrmions can coexist [18,53]. While the single-band model discussed in this work cannot explain such a coexistence, the extension of the key concept to realistic multiband electronic Hamiltonians may describe such observations.

Interestingly, there is a simple way to find out if the effective tight-binding model for a given metal has a relative sign difference between hopping parameters along different directions. If the maximum or the minimum of the relevant energy bands that cross the Fermi level lies at the  $\Gamma$  point, then all hoppings have the same sign. This observation, together with the results discussed so far, leads to a very important general conjecture. Materials that host Bloch skyrmions should not have the maximum or minimum of the relevant bands without SOC at the  $\Gamma$  point. We could identify many materials that host Bloch skyrmions and have their band extremum away from the  $\Gamma$  point [41–44]. Similarly, Neel skyrmions are more likely when the maximum or the minimum lies at the  $\Gamma$  point, and on surfaces or interfaces so that Rashba effect is dominant. Once again, this condition seems to hold for many Neel skyrmion hosts [54–56]. It is also important to note that

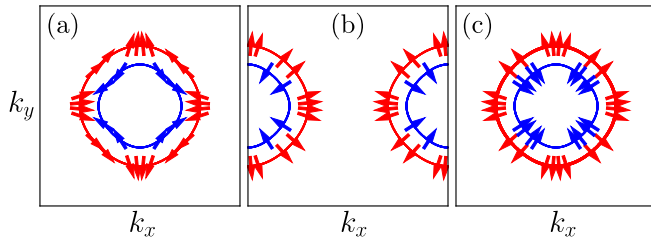


FIG. 5. Spin textures in the momentum space on Fermi contours at  $1/5$  filling for (a) Dresselhaus SOC strength  $\lambda = 0.3$  and  $t_x = t_y = 1.0$ , (b)  $\lambda = 0.3$ ,  $t_x = -1.0$ ,  $t_y = 1.0$ , and (c) Dresselhaus SOC strength  $\lambda$  having an extra minus sign along the  $x$  direction leading to a lattice version of the  $\sigma \cdot \mathbf{k}$  model with  $t_x = t_y = 1.0$ . In all panels only the first Brillouin zones are displayed.

a large number of skyrmion-host metals have a complicated band structure with a large number of bands crossing the Fermi level. Therefore, it may not be straightforward to test the above condition for such materials. In principle, it would be very interesting to write a multiband version of the present theory to allow predictions for a wider class of materials.

Finally, we discuss a connection with skyrmions in Weyl semimetals. The Hamiltonian Eq. (1) for  $J_H = 0$  can be easily diagonalized. The spin-momentum locking leads to well-defined spin textures in the momentum space (see Fig. 5). From our results we conclude that the nature of the momentum-space spin textures completely determines the nature of the real-space magnetic texture that appear when Hund's or Hubbard interactions are included. Spin textures on the Fermi contours for Hamiltonian Eq. 1 at  $J_H = 0$  display a specific antiskyrmion-like pattern [see Fig. 5(a)]. These results are consistent with an earlier prediction based on symmetry analysis of different type of SOC terms included in a continuum model [52,57]. However, our tight-binding description allows to relate the type of textures to specific features in the band structure, which is accessible via realistic *ab initio* calculations.

If the sign of one of the hopping terms is reversed then the momentum-space spin textures attain a Neel-skyrmion-like pattern, but away from the  $\Gamma$  point [see Fig. 5(b)]. Finally, introducing a relative sign in the SOC coupling  $\lambda$  along  $x$  and  $y$  directions leads to a Neel-skyrmion-like pattern centered at the  $\Gamma$  point [see Fig. 5(c)]. In all cases, the real-space magnetic textures are such that the spin directions around the core are orthogonal to the momentum space spin directions.

We further emphasize the importance of the effective spin Hamiltonian in providing a general understanding of the interrelation among the nature of topological magnetic textures, the relative sign of the hopping parameters, and the type

of SOC. In the starting electronic Hamiltonian Eqs. (1) and (2), the hopping and the SOC parameters belong to independent terms. However, the effective Hamiltonian brings these parameters together in the form of an explicit DM-like interaction. It is this  $t\lambda$  term in Eqs. (7) and (8) that facilitates a general understanding of the relation between relative sign change in  $x$ - and  $y$ -direction hoppings and the types of magnetic textures. In a two-dimensional tight-binding model, the same sign for  $t_x$  and  $t_y$  leads to an extremum at the  $\Gamma$  point. Therefore, a relative sign change is easily detected as location of band extremum away from the  $\Gamma$  point.

We also note that a change in sign of SOC strength  $\lambda$  along one direction transform the continuum version of the Dresselhaus Hamiltonian  $\lambda(\sigma^x k_x - \sigma^y k_y)$  form to Weyl semimetal  $\lambda(\sigma \cdot \mathbf{k})$ . Therefore, the Weyl semimetals that are described by the  $\sigma \cdot \mathbf{k}$  Hamiltonian should naturally lead to Bloch skyrmions [37]. Once again, it is the  $t\lambda$  term in the effective Hamiltonian that connects directly the magnetism of Dresselhaus and Weyl Hamiltonians. Therefore, our results are directly relevant for understanding the ground states of magnetic Weyl semimetals.

## V. CONCLUSION

A number of antiskyrmion host materials, such as  $\text{Mn}_{1.4}\text{Pt}_{0.9}\text{Pd}_{0.1}\text{Sn}$ ,  $\text{Mn}_{1.4}\text{PtSn}$ , and  $\text{Mn}_2\text{Rh}_{0.95}\text{Ir}_{0.05}\text{Sn}$ , happen to be inverse Heusler metals lacking a center of inversion [15–17]. The presence of a magnetic ion together with heavy elements suggests that an appropriate description of the magnetism of these materials can be in terms of a double exchange model modified by Dresselhaus SOC. We establish this by explicitly showing that magnetic Dresselhaus metals support nanoscale antiskyrmions. An understanding of the stability of antiskyrmions is achieved in terms of a conventional spin-only model derived from the microscopic DDE Hamiltonian. We provide a recipe for turning antiskyrmions into Bloch skyrmions, and thereby providing a novel connection between the type of topological magnetic textures and the underlying electronic band structure. Such a connection will be completely missed in a spin-only model written without reference to a starting microscopic model. We also discuss the connection between the  $\sigma \cdot \mathbf{k}$  model typically used to describe Weyl semimetals and the hopping-sign modified Dresselhaus Hamiltonian. This connection supports the experimental studies of skyrmions in magnetic Weyl semimetals [37–40] and puts forward a clear recipe for design of new skyrmion-host materials.

## ACKNOWLEDGMENT

We acknowledge the use of the computing facility at IISER Mohali.

- [1] A. Fert, N. Reyren, and V. Cros, *Nat. Rev. Mater.* **2**, 17031 (2017).
- [2] R. Wiesendanger, *Nat. Rev. Mater.* **1**, 16044 (2016).
- [3] A. Fert, V. Cros, and J. Sampaio, *Nat. Nanotechnol.* **8**, 152 (2013).

- [4] N. Nagaosa and Y. Tokura, *Nat. Nanotechnol.* **8**, 899 (2013).
- [5] A. N. Bogdanov and C. Panagopoulos, *Phys. Today* **73**(3), 44 (2020).
- [6] X. Z. Yu, N. Kanazawa, Y. Onose, K. Kimoto, W. Z. Zhang, S. Ishiwata, Y. Matsui, and Y. Tokura, *Nat. Mater.* **10**, 106 (2011).

- [7] S. Meyer, M. Perini, S. von Malottki, A. Kubetzka, R. Wiesendanger, K. von Bergmann, and S. Heinze, *Nat. Commun.* **10**, 3823 (2019).
- [8] P.-J. Hsu, L. Rózsa, A. Finco, L. Schmidt, K. Palotás, E. Vedmedenko, L. Udvardi, L. Szunyogh, A. Kubetzka, K. von Bergmann *et al.*, *Nat. Commun.* **9**, 1571 (2018).
- [9] A. Tonomura, X. Yu, K. Yanagisawa, T. Matsuda, Y. Onose, N. Kanazawa, H. S. Park, and Y. Tokura, *Nano Lett.* **12**, 1673 (2012).
- [10] X. Yu, W. Koshibae, Y. Tokunaga, K. Shibata, Y. Taguchi, N. Nagaosa, and Y. Tokura, *Nature (London)* **564**, 95 (2018).
- [11] T. Nagase, M. Komatsu, Y. So, T. Ishida, H. Yoshida, Y. Kawaguchi, Y. Tanaka, K. Saitoh, N. Ikarashi, M. Kuwahara, and M. Nagao, *Phys. Rev. Lett.* **123**, 137203 (2019).
- [12] N. Romming, C. Hanneken, M. Menzel, J. E. Bickel, B. Wolter, K. von Bergmann, A. Kubetzka, and R. Wiesendanger, *Science* **341**, 636 (2013).
- [13] X. Yu, N. Kanazawa, W. Zhang, T. Nagai, T. Hara, K. Kimoto, Y. Matsui, Y. Onose, and Y. Tokura, *Nat. Commun.* **3**, 988 (2012).
- [14] X. Zhao, C. Jin, C. Wang, H. Du, J. Zang, M. Tian, R. Che, and Y. Zhang, *Proc. Natl. Acad. Sci. USA* **113**, 4918 (2016).
- [15] A. K. Nayak, V. Kumar, T. Ma, P. Werner, E. Pippel, R. Sahoo, F. Damay, U. K. Röbber, C. Felser, and S. S. P. Parkin, *Nature (London)* **548**, 561 (2017).
- [16] P. Vir, N. Kumar, H. Borrmann, B. Jamijansuren, G. Kreiner, C. Shekhar, and C. Felser, *Chem. Mater.* **31**, 5876 (2019).
- [17] J. Jena, R. Stinshoff, R. Saha, A. K. Srivastava, T. Ma, H. Deniz, P. Werner, C. Felser, and S. S. P. Parkin, *Nano Lett.* **20**, 59 (2020).
- [18] L. Peng, R. Takagi, W. Koshibae, K. Shibata, K. Nakajima, T.-H. Arima, N. Nagaosa, S. Seki, X. Yu, and Y. Tokura, *Nat. Nanotechnol.* **15**, 181 (2020).
- [19] M. Hoffmann, B. Zimmermann, G. P. Müller, D. Schürhoff, N. S. Kiselev, C. Melcher, and S. Blügel, *Nat. Commun.* **8**, 308 (2017).
- [20] S. Hayami and Y. Motome, *Phys. Rev. Lett.* **121**, 137202 (2018).
- [21] S. Hayami and Y. Motome, *Phys. Rev. B* **99**, 094420 (2019).
- [22] Z. Wang, Y. Su, S.-Z. Lin, and C. D. Batista, *Phys. Rev. Lett.* **124**, 207201 (2020).
- [23] A. V. Bezvershenko, A. K. Kolezhuk, and B. A. Ivanov, *Phys. Rev. B* **97**, 054408 (2018).
- [24] S. Hayami and R. Yambe, *J. Phys. Soc. Jpn.* **90**, 073705 (2021).
- [25] L. Jin, B. Xi, J.-W. Mei, and Y. Liu, [arXiv:2106.00207](https://arxiv.org/abs/2106.00207).
- [26] J. P. Chen, D.-W. Zhang, and J. M. Liu, *Sci. Rep.* **6**, 29126 (2016).
- [27] U. K. Roessler, A. Bogdanov, and C. Pfleiderer, *Nature (London)* **442**, 797 (2006).
- [28] N. Mohanta, E. Dagotto, and S. Okamoto, *Phys. Rev. B* **100**, 064429 (2019).
- [29] J. Iwasaki, A. J. Beekman, and N. Nagaosa, *Phys. Rev. B* **89**, 064412 (2014).
- [30] S. D. Yi, S. Onoda, N. Nagaosa, and J. H. Han, *Phys. Rev. B* **80**, 054416 (2009).
- [31] S. Huang, C. Zhou, G. Chen, H. Shen, A. K. Schmid, K. Liu, and Y. Wu, *Phys. Rev. B* **96**, 144412 (2017).
- [32] L. Qiu, J. Xia, Y. Feng, L. Shen, F. J. Morvan, X. Zhang, X. Liu, L. Xie, Y. Zhou, and G. Zhao, *J. Magn. Magn. Mater.* **496**, 165922 (2020).
- [33] W. Koshibae and N. Nagaosa, *Nat. Commun.* **7**, 10542 (2016).
- [34] D. S. Kathyat, A. Mukherjee, and S. Kumar, *Phys. Rev. B* **102**, 075106 (2020).
- [35] D. S. Kathyat, A. Mukherjee, and S. Kumar, *Phys. Rev. B* **103**, 035111 (2021).
- [36] T. Okubo, S. Chung, and H. Kawamura, *Phys. Rev. Lett.* **108**, 017206 (2012).
- [37] Y. Araki, *Ann. Phys. (Leipzig)* **532**, 1900287 (2020).
- [38] H. Wu, P. Sun, D. Hsieh, H. Chen, D. C. Kakarla, L. Deng, C.-W. Chu, and H. Yang, *Mater. Today Phys.* **12**, 100189 (2020).
- [39] P. Puphal, V. Pomjakushin, N. Kanazawa, V. Ukleev, D. J. Gawryluk, J. Ma, M. Naamneh, N. C. Plumb, L. Keller, R. Cubitt, E. Pomjakushina, and J. S. White, *Phys. Rev. Lett.* **124**, 017202 (2020).
- [40] M. Redies, F. R. Lux, J.-P. Hanke, P. M. Buhl, S. Blügel, and Y. Mokrousov, *Phys. Rev. B* **102**, 184407 (2020).
- [41] K. V. Shanavas and S. Satpathy, *Phys. Rev. B* **93**, 195101 (2016).
- [42] H. Choi, Y.-Y. Tai, and J.-X. Zhu, *Phys. Rev. B* **99**, 134437 (2019).
- [43] T. Nomoto, T. Koretsune, and R. Arita, *Phys. Rev. Lett.* **125**, 117204 (2020).
- [44] T. Koretsune, N. Nagaosa, and R. Arita, *Sci. Rep.* **5**, 13302 (2015).
- [45] I. Martin and C. D. Batista, *Phys. Rev. Lett.* **101**, 156402 (2008).
- [46] K. Pasrija and S. Kumar, *Phys. Rev. B* **93**, 195110 (2016).
- [47] S. Kumar and P. Majumdar, *Eur. Phys. J. B* **50**, 571 (2006).
- [48] A. Mukherjee, N. D. Patel, C. Bishop, and E. Dagotto, *Phys. Rev. E* **91**, 063303 (2015).
- [49] R. Keesman, A. O. Leonov, P. van Dieten, S. Buhardt, G. T. Barkema, L. Fritz, and R. A. Duine, *Phys. Rev. B* **92**, 134405 (2015).
- [50] S. Banerjee, J. Rowland, O. Erten, and M. Randeria, *Phys. Rev. X* **4**, 031045 (2014).
- [51] M. N. Wilson, A. B. Butenko, A. N. Bogdanov, and T. L. Monchesky, *Phys. Rev. B* **89**, 094411 (2014).
- [52] U. Güngördü, R. Nepal, O. A. Tretiakov, K. Belashchenko, and A. A. Kovalev, *Phys. Rev. B* **93**, 064428 (2016).
- [53] K. Karube, L. Peng, J. Masell, X. Yu, F. Kagawa, Y. Tokura, and Y. Taguchi, *Nat. Mater.* **20**, 335 (2021).
- [54] K. Xu and H. J. Xiang, *Phys. Rev. B* **92**, 121112(R) (2015).
- [55] S. Bhowal and S. Satpathy, *npj Comput. Mater.* **5**, 61 (2019).
- [56] S. Bhowal and S. Satpathy, *Phys. Rev. B* **99**, 245145 (2019).
- [57] S.-J. Lee, K.-W. Kim, H.-W. Lee, and K.-J. Lee, *J. Magn. Magn. Mater.* **455**, 14 (2018).